The Effect of Smoke Particles on Clouds and Climate Forcing

Yoram J. Kaufman* and Robert S. Fraser

Smoke particles from biomass burning can generate forcing of climate by modifying cloud microphysics and reflectance of sunlight. Cloud modification, critical to an understanding of climate change, is uncertain and variable. Satellite data over the Amazon Basin and Cerrado were analyzed for cloud reflectance and droplet size and for smoke concentration. Smoke increased cloud reflectance from 0.35 to 0.45, while reducing droplet size from 14 to 9 micrometers. The regional variability of the smoke effect was correlated to the availability of water vapor. During the 3 months of biomass burning in the dry season, the smoke-cloud forcing of climate was only −2 watts per square meter in this region, much smaller than what can be inferred from model predictions.

Cloud modification by aerosol particles (*1*, *2*) may be the missing process in reconciling climate models with observations (*3*). Yet the chemical and physical processes involved may be too complex for parameterization in climate models (*4*), and some generalization is needed. Large-scale observations of the relation between cloud properties, the surrounding aerosol, and meteorological parameters represent one way to achieve a quantification of the aerosol impact on cloud radiative properties and climate forcing. We report observations that confirm the effect of aerosol particles on cloud microphysical and radiative properties and quantify the dependence of this effect on the availability of total precipitable water vapor. The results, if not disproved in other cases, may form the basis for understanding the aerosol-cloud interaction as a first step for use in climate models.

Smoke aerosol particles generated from biomass-burning fires in the tropics (*5*) can affect atmospheric radiation (*6*) and climate directly by reflecting sunlight back to space (*3*). This effect was shown recently to be relatively small (*7*). Aerosol can also force climate indirectly by modifying cloud microphysics and reflectivity (*2*, *8*). Smoke particles generated by fires and modified in the lower troposphere (*9*, *10*) are effective cloud condensation nuclei (CCN) (*11*) and have been shown to increase the concentration of cloud droplets (*11–13*). Here we show that smoke particles also increase the reflectance of thin or moderately thick clouds.

Measurements by satellite sensors, like the Advanced Very High Resolution Radiometer (AVHRR), allow derivation of cloud droplet size and reflectance and of the smoke optical thickness (a measure of smoke concentration) in cloud-free regions (*13*). The relation between the cloud properties and the optical thickness of the aerosol can then be used to quantify smoke-cloud interaction. But measurements of this interaction from satellites may be complicated by the variability of the smoke particle size distribution, its hygroscopicity, and the presence of absorbing black carbon and cloud dynamics (*4*). Optical thickness is sensitive not only to the smoke concentration but also to the aerosol particle size. Large variability in the aerosol particle size can therefore reduce the correlation between the concentration of CCNs that determine cloud properties and the satellite-derived smoke optical thickness. However, for smoke, the median mass radius r_m of the size distribution varies only by $\Delta r_m = \pm 0.02$ μm ($r_m \sim 0.14$ μm) for South American (*14*), African (*15*), and North American fires (*9*). This corresponds to an uncertainty of 35% in deriving the concentration for particles with radius ≥0.05 μm that are efficient CCNs. This relatively small uncertainty has also been confirmed by recent direct measurements of CCN in Brazil and Africa (*16*). The large coverage of AVHRR observations of smoke-cloud interaction for thousands of clouds reduces the uncertainty in measuring the effect of smoke on clouds.

In a previous study (*13*), remote sensing of smoke and cloud properties over tropical South America, by means of AVHRR satellite data with 1-km resolution, showed that smoke reduces the effective cloud-droplet radius R_d from 15 to 8 μm, but decreases the cloud reflectance from 0.71 to 0.68 due to absorption of sunlight by black carbon that is part of the smoke. Only bright clouds that are strongly affected by black carbon were used (*17*, *18*), thus obscuring the effect of CCNs on cloud reflectance (*13*). To detect the effect of smoke on more typical clouds [reflectance ~0.45 (*19*)] that are susceptible to the smoke CCN effect (*20*), we used a sensitive cloud-detection scheme. For a 1° by 1° latitude-longitude grid, low clouds that are embedded in the smoke layer [apparent temperature (*21*) ≥ 270 K] were selected by their reflectance at 0.64 μm, ρ_{cv} (cv, cloud-visible wavelength), and the difference between the apparent temperature at 3.7 μm, T_4, and at 11 μm, T_{11}:

$$270\ K \le T_{11} \le 290\ K,\ \rho_{cv} \ge 0.2,\ \text{and}$$

$$T_4 - T_{11} > 8\ K \qquad (1)$$

The thresholds are appropriate for the AVHRR apparent surface temperature of 297 ± 1 K (Table 1), for a cloud-free surface plus smoke reflectance at 0.64 μm of <0.2, and for a small difference of ($T_4 - T_{11}$) for cloud-free regions and a large value for clouds. By including clouds with reflectance ρ_{cv} down to $\rho_{cv} = 0.2$, the average cloud reflectance of 0.7 in the previous study (*13*) was reduced to the range of 0.35 to 0.45.

Eleven AVHRR images, collected at 3:30 p.m. local time in August and September 1987 over the Amazon Basin and Cerrado (20°S to 5°N and 55°W to 70°W), were analyzed for view angles ≤30°. For each 1° by 1° grid box, the AVHRR measurements were used to derive the average cloud reflectances at 0.64 μm, ρ_{cv}, and 3.7 μm, ρ_{c4} (the number 4 refers to the 3.7-μm channel), and in cloud-free regions the average smoke optical thickness in the grid box, τ_s (*22*). The cloud droplet radius R_d is derived from ρ_{c4} with the use of a radiative transfer look-up table (*13*, *23*).

The dependence of the cloud properties on τ_s was explored for four latitude zones. The droplet size decreases, and the cloud reflectance increases, with τ_s for the three northern zones for moderate smoke ($0.2 \le \tau_s \le 0.8$) (Fig. 1). For the Cerrado region (the southernmost zone, 11°S to 20°S), the effect is smallest. The effect of smoke on cloud droplet size is similar for the four cloud-top temperature ranges investigated here (Fig. 2). For moderate smoke the effect on the droplet size increases with latitude northward, associated with an increase in precipitable water vapor. The effect of smoke on cloud reflectance is linearly related to the cloud droplet size (Fig. 3). For heavy smoke ($0.8 \le \tau_s \le 1.3$) the effect on droplet size is small as a result of saturation of the smoke effect (Table 2). Similar to sulfate aerosol (*24*), an increase in the smoke aerosol concentration above a given threshold cannot generate additional droplets because of limited availability of liquid water (*25*).

These results were compared with a simple model based on the study by Twomey (*26*). For fixed cloud liquid water content,

Laboratory for Atmospheres (913), NASA Goddard Space Flight Center, Greenbelt, MD 20771, USA.

*To whom correspondence should be addressed. E-mail: kaufman@climate.gsfc.nasa.gov

Table 1. Statistical information on the four zones of the analysis. The minimum and average smoke optical thickness, the fraction of low clouds, and their average size are derived from the 1° by 1° analyzed AVHRR data. The total precipitable water vapor (W) and the lapse rate are derived from the average of radiosonde measurements in each of thezones for the timeof the satellite data (*22*). The lapse rate is the rate of decrease of air temperature with altitude. T_{11} and T_{11s} are the apparent cloud and surface temperatures, respectively, as measured from the satellite. The value of T_{11s} after correction for atmospheric effects is indicated.

Latitude zone (°)	Smoke optical thickness		Fraction of low cloud ($T_{11} \geq 270°$)	Average cloud size (km²)		W (cm)	Solar zenith angle (°)	Surface temp. (K)		Lapse rate (K/km)
	Minimum	Average		Number weighted	Area weighted			T_{11s}	Corr. for water vapor	
5N–0	0.17	0.31	0.09	5.3	580	4.5–5.0	51	296	302	4.5 ± 0.2
0–5S	0.21	0.50	0.12	5.9	800	3.5–4.5	53	297	302	5.5 ± 0.8
5–11S	0.32	0.92	0.11	4.5	150	3.0–4.0	55	297	301	6.6 ± 2
11–20S	0.21	1.13	0.16	6.9	400	2.5–3.5	58	296	300	3.7 ± 1

aerosol size distribution, cloud structure, and dynamics, and assuming the number of CCNs is proportional to τ_s, the relation between the cloud droplet concentration N_d and CCN is

$$N_d/N_{do} = (CCN/CCN_o)^{0.7} = (\tau_s/\tau_{so})^{0.7} \quad (2)$$

and

$$R_d/R_{do} = (\tau_s/\tau_{so})^{-\alpha}, \alpha = 0.7/3 = 0.23 \quad (3)$$

where the subscript o stands for the background conditions defined for $\tau_{so} = 0.2$. The model results fit the measured droplet size for precipitable water vapor W of ~4 cm, overestimate it for $W < 4$ cm, and underestimate it for $W > 4$ cm (Figs. 2 and 3).

Model predictions for ρ_{cv} were based on radiative transfer calculations for plane-parallel clouds with optical thickness τ_c and single-scattering albedo ω_c. For fixed liquid water content (*26*)

$$\tau_c/\tau_{co} = (R_d/R_{do})^{-1} \quad (4)$$

ω_c was computed assuming that the cloud absorption is equal to the smoke column absorption (*13*):

$$\omega_c = [\tau_c - (1 - \omega_s)\tau_s]/\tau_c \quad (5)$$

where ω_s is the smoke single-scattering albedo. Best agreement with the measurements for moderate smoke is obtained when $\omega_s > 0.9$ (Figs. 1 to 3), higher than the reported value (*6*, *7*, *9*, *18*) of 0.85 to 0.90. This discrepancy may result from a smaller fraction of the smoke column interacting with the cloud, or an increase in the cloud liquid water with an increase in the smoke concentration. The best fit for heavy smoke (Table 2) is obtained for $\omega_s = 0.85$ to 0.90, similar to the fit for bright clouds in the earlier study (*13*).

There are other factors that could con-

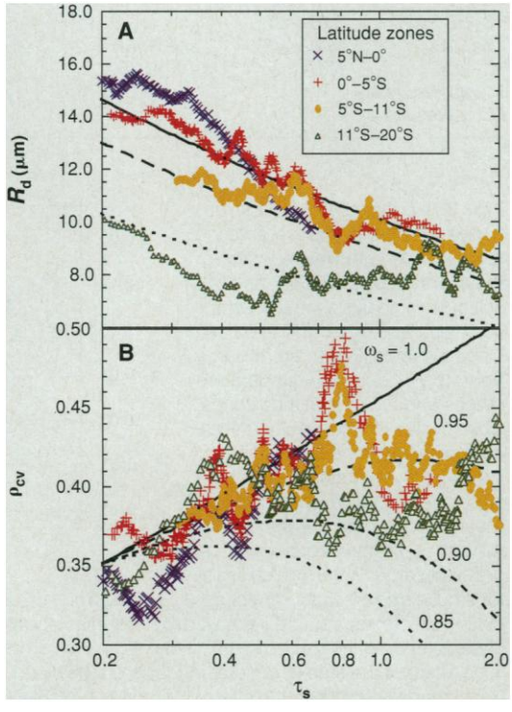

Fig. 1. Twenty-point running averages showing (**A**) the decrease in the cloud droplet radius R_d and (**B**) an increase in the cloud reflectance of sunlight ρ_{cv} at 0.64 μm as a function of the smoke optical thickness τ_s, analyzed from AVHRR satellite data for the four latitude zones in South America. Model predictions (*26*) are given by black lines. For the cloud droplet size, the model lines are for several initial values of R_{do}, defined in Eq. 3 and given on the ordinate for $\tau_s = 0.2$. For the cloud reflectance, the lines are for several values of the smoke single-scattering albedo ω_s. There is no dependence of R_d on ω_s. Only low clouds with cloud-top temperature detected by the satellite at 11 μm, T_{11}, 290 K > T_{11} > 285 K, were included in the analysis. The view direction was restricted to ±30°.

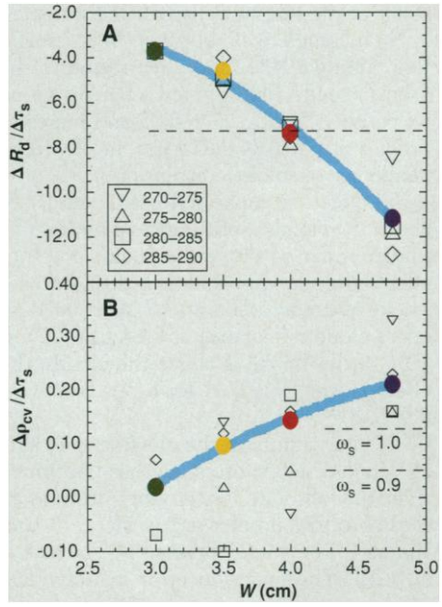

Fig. 2. (**A**) Rate of decrease in the cloud droplet size $\Delta R_d/\Delta\tau_s$ and (**B**) rate of increase in cloud reflectance $\Delta\rho_{cv}/\Delta\tau_s$ resulting from a change in the smoke concentration, given by the optical thickness τ_s in the range $0.2 \leq \tau_s \leq 0.8$. The results are calculated from the data in Fig. 1, and for other ranges of cloud-top temperatures as indicated by the empty symbols. Color circles are weighted averages of the results for the four cloud-top temperatures. They were weighted by the number of data points in each temperature range. The colors correspond to the plots for different latitude ranges of Fig. 1 that are here translated to the value of the total precipitable water vapor W with the data from Table 1. The blue curve is a smooth fit to the color circles. Model results for $\Delta R_d/\Delta\tau_s$ and for $\Delta\rho_{cv}/\Delta\tau_s$, in which two values are used of the smoke single-scattering albedo ω_s, are given by the dashed lines.

tribute to a change in the cloud droplet size and cloud reflectance, thus introducing uncertainty in the conclusions:

1) Random noise and natural variability. Each point in Fig. 1 averages data from an area 200,000 km^2 taken from 20 different locations, and therefore residual errors and natural variability in the aerosol size distribution and cloud properties, uncertainty in the surface reflectance, and instrumental noise are expected to be small.

2) Variations in the cloud-top temperature. Averaging on layers of cloud-top temperature with 5-K increments reduces the variability to $\Delta T_{11} = \pm 0.1$ K, corresponding to only a small uncertainty in the cloud reflectance (*19*) and droplet size.

3) Variation in the view direction. The data were selected for view angles $-30° \geq \theta \geq 30°$. Anisotropic cloud reflectance can cause substantial variability in derived cloud properties (*19*). Repeating the analysis for only $\theta = \pm 10°$ resulted in similar cloud droplet size. The data for cloud reflectance were too noisy in this instance as a result of the substantially reduced statistics.

4) Incomplete cloud cover. We estimate that adding a 10% cloud-free region to the 1-km^2 cloudy field-of-view changes cloud reflectivity by $\Delta\rho_{cv} \sim -0.03$ and increases droplet size by $\Delta R_d \sim 0.5$ μm, mostly independently of smoke concentration.

5) Effect of smoke reflectance under or above the clouds. Reflectance of sunlight by smoke under or above the clouds does not affect the derived droplet size, because smoke is transparent at 3.7 μm, but can affect cloud reflectance at 0.64 μm (*27*). If 10% of the smoke is above the clouds, the effect is $\Delta\rho_{cv} \sim -0.01$ for $\rho_{cv} = 0.4$, $\omega_s = 0.9$, and $\tau_s = 0.8$.

6) Uncertainty in the cloud droplet size. A detailed sensitivity study has confirmed that the absolute uncertainty in remote sensing of the droplet size is $\Delta R_d \sim 3$ μm, similar to the value obtained by Platnick *et al.* (*20*). The precision error in individual measurements is expected to be $\Delta R_d \sim 0.3$ μm for a cloud-top temperature of 270 K, increasing to $\Delta R_d \sim 1.5$ μm for 290 K. The averaging process is expected to decrease the error in R_d by a factor of 2 to 5.

The results confirm that smoke increases the reflectance of sunlight by clouds and therefore generates an indirect forcing of climate; the effect is variable and insignificant in the drier Cerrado. The variability of the effect with latitude is correlated with the precipitable water vapor W, in good agreement with Twomey's model for $W = 4$ cm. Other atmospheric and surface parameters also vary with latitude (Table 1), but not as systematically as W. No relation was established between the variability of the smoke effect and the cloud type (indicated by the cloud average size), in contrast to the finding for sulfate aerosol (*28*). Reduction of available water vapor may decrease the latent heat released during updraft and thereby reduce the updraft velocity and the fraction of activated smoke particles (*25*), thus reducing the impact of the increase in the smoke concentration on the reduction in cloud droplet size and increase in the cloud reflectance. Leaitch *et al.* (*29*) also detected variability of the aerosol effect (sulfates in their study) on clouds. They found, from aircraft in situ measurements, that the aerosol effect on clouds is larger for lightly turbulent air than for smooth air, possibly also as a result of a smaller updraft in the smooth air.

Biomass burning occurs during 3 months of the dry season (July through September) with strong anticyclonic subsidence that often suppresses convection (*30*) and reduces low cloud coverage (Table 1). For the average smoke effect on cloud reflectance $\Delta\rho_{cv}/\Delta\tau_s = 0.12 \pm 0.08$ for moderate smoke, the increase in the cloud reflectance is $\Delta\rho_{cv} = 0.07 \pm 0.05$. The total regional albedo is the product of the cloud fraction and $\Delta\rho_{cv}$, which is $\sim 0.01 \pm 0.007$. The corresponding cloud radiative forcing (*4*) is -2 ± 1 W/m^2. The biggest uncertainty in this estimate is in the background value of τ_s. If we used $\tau_{so} = 0.1$ instead of 0.2, it would double the forcing. Because this analysis is for a region with maximum smoke loading, a forcing of -2 W/m^2 is surprisingly small. Previous estimates (*2*) of indirect smoke forcing of -1 W/m^2 are for a global annual average as a result of smoke generated in the tropics during ~3 months per year. This would require a forcing of -20 W/m^2 during the 3 months of biomass burning in the 25° latitude belt where most smoke is generated, a requirement 10 times that of the present result (*31*). The small indirect smoke forcing of climate and the small direct forcing reported earlier (*7*) for South America may be the reason why smoke aerosol provides a weaker signal than sulfate aerosol in the temperature records (*32*).

Satellite remote sensing of the aerosol effect on clouds will be enhanced in 1998 with the launch of the MODIS (MODerate

Table 2. Summary of the analysis of the AVHRR satellite data for the rate of change in the cloud droplet size ΔR_d and reflectance $\Delta\rho_{cv}$ with a change in the smoke optical thickness τ_s, taken from Fig. 2. The average results are given for each latitude zone, with the associated total precipitable water vapor W for two ranges of τ_s: moderate smoke, $0.2 \leq \tau_s \leq 0.8$; and heavy smoke, $0.8 \leq \tau_s \leq 1.3$. The results are averaged on the four cloud-top temperatures. There is a significantly smaller effect of smoke on cloud droplet size for $0.8 \leq \tau_s \leq 1.3$ and a resulting decrease rather than increase in the cloud reflectance for this range of τ_s. The model results are also given for $\omega_s = 1.0$ and 0.9.

Latitude zone (°)	W (cm)	$\Delta R_d/\Delta\tau_s$		$\Delta\rho_{cv}/\Delta\tau_s$	
		$0.2 \leq \tau_s \leq 0.8$	$0.8 \leq \tau_s \leq 1.3$	$0.2 \leq \tau_s \leq 0.8$	$0.8 \leq \tau_s \leq 1.3$
5N–0	4.5–5.0	−11.2	–	0.21	–
0–5S	3.5–4.5	−7.3	−1.1	0.14	−0.15
5–11S	3.0–4.0	−4.8	−3.5	0.10	−0.08
11–20S	2.5–3.5	−3.7	0.7	0.02	−0.03
Model results $\omega_s = 1$		−7.3	−2.8	0.13	0.05
Model results $\omega_s = 0.9$		−7.3	−2.8	0.05	−0.02

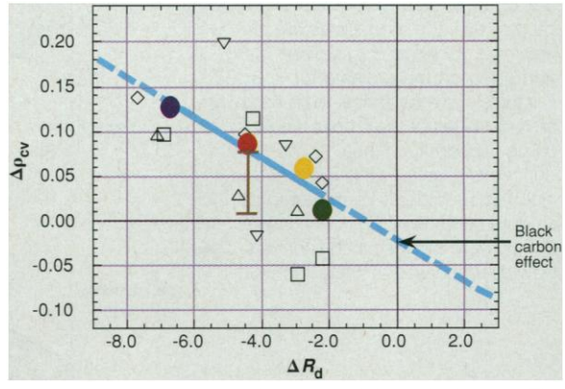

Fig. 3. Relation between the enhancement in the cloud reflectance of sunlight $\Delta\rho_{cv}$ and the reduction of the cloud droplet size ΔR_d as a result of an increase in the smoke optical thickness τ_s from 0.2 to 0.8. Open symbols (Fig. 2) are for data from four cloud-top temperature ranges and the four latitude zones. Color circles are the weighted averages for each zone, with the color indicating the latitude of zones as in Figs. 1 and 2. The aqua line is a linear fit to the data; it is extrapolated with a dashed aqua line. The gray vertical bar is the model results for smoke single-scattering albedo ω_s, varying from 1.0 at the top of the bar to 0.85 at the bottom. The cloud reflectance can be increased by the effect of the smoke-induced CCNs and decreased by absorption by black carbon in the smoke. When the droplet size does not change ($\Delta R_d/\Delta\tau_s = 0$), there is no effect of the smoke-generated CCNs on the cloud properties. In this instance, ρ_{cv} decreased by 0.024 (arrow), indicating the effect of absorption by black carbon on the cloud reflectance.

resolution Imaging Spectroradiometer) sensor on the Earth Observing System satellite. MODIS provides an enhanced remote-sensing capability (*33*) that will enable precise monitoring not only of the interaction of smoke with clouds but also of the spatial distribution of precipitable water vapor, presently available only from sparse radiosonde data. At that time, testing the hypothesized impact of water vapor on the smoke-cloud interaction will be possible.

REFERENCES AND NOTES

1. A. Jones, D. L. Roberts, A. Slingo, *Nature* **370**, 450 (1994).
2. J. E. Penner, R. E. Dickinson, C. A. O'Neill, *Science* **256**, 1432 (1992).
3. J. Hansen, M. Sato, A. Lacis, R. Ruedy, *Philos. Trans. R. Soc. London Ser. B* **352**, 231 (1997).
4. S. E. Schwartz *et al.*, in *Aerosol Forcing of Climate*, R. J. Charlson and J. Heintzenberg, Eds. (Wiley, Chichester, UK, 1995), pp. 251–280.
5. P. J. Crutzen and M. O. Andreae, *Science* **250**, 1669 (1990); A. W. Setzer and M. C. Pereira, *Ambio* **20**, 19 (1991); P. Artaxo, F. Gerab, M. A. Yamasoe, J. V. Martins, *J. Geophys. Res.* **99**, 22857 (1994); W. M. Hao and M.-H. Liu, *Global Biogeochem. Cycles* **8**, 495 (1994).
6. Y. J. Kaufman *et al.*, *J. Geophys. Res.* **97**, 14581 (1992).
7. P. V. Hobbs, J. S. Reid, R. A. Kotchenruther, R. J. Ferek, R. Weiss, *Science* **275**, 1776 (1997).
8. S. Twomey, M. Piepgrass, T. L. Wolfe, *Tellus* **36b**, 356 (1984); P. V. Hobbs, in *Aerosol-Cloud-Climate Interactions*, P. V. Hobbs, Ed. (Academic Press, New York, 1993), p. 33.
9. L. F. Radke *et al.*, *Global Biomass Burning* (MIT Press, Cambridge, MA, 1991), p. 209.
10. C. Liousse, C. Devaux, F. Dulac, H. Cachier, *J. Atmos. Chem.* **22**, 1 (1995).
11. J. Warner and S. Twomey, *J. Atmos. Sci.* **24**, 704 (1967); P. V. Hobbs and L. F. Radke, *Science* **163**, 279 (1969); J. G. Hudson, J. Hallett, C. F. Rogers, *J. Geophys. Res.* **96**, 10847 (1991).
12. D. A. Hegg, L. F. Radke, P. V. Hobbs, *J. Geophys. Res.* **96**, 18727 (1991); W. R. Leaitch, J. W. Strapp, G. A. Isaac, J. G. Hudson, *Tellus* **38B**, 328 (1986).
13. Y. J. Kaufman and T. Nakajima, *J. Appl. Meteorol. Squires Spec. Issue* **32**, 729 (1993).
14. L. A. Remer, Y. J. Kaufman, B. N. Holben, *Global Biomass Burning*, J. Levin, Ed. (MIT Press, Cambridge, MA, 1996), p. 519.
15. M. O. Andreae *et al.*, *J. Geophys. Res.* **99D**, 12793 (1994); P. Artaxo, F. Gerab, M. A. Yamasoe, J. V. Martins, in (*14*), p. 519.
16. P. Le Canut *et al.*, *J. Geophys. Res.* **101**, 23615 (1996); B. E. Anderson *et al.*, *ibid.*, p. 24117.
17. H. Cachier, M. P. Bremond, P. Buat-Ménard, *Nature* **340**, 371 (1989).
18. C. Liousse *et al.*, *J. Chem.* **22**, 1 (1996).
19. J. A. Coakley Jr. and R. Davies, *J. Atmos. Sci.* **43**, 1025 (1986); J. A. Coakley Jr., *Tellus* **43B**, 420 (1991).
20. S. Platnick and S. Twomey, *J. Appl. Meteorol.* **33**, 334 (1994); S. Platnick and F. P. J. Valero, *J. Atmos. Sci.* **52**, 2985 (1995).
21. Apparent temperature is derived from the radiance at 11 μm measured by the satellite, T_{11}. It is lower by a few degrees kelvin than the actual temperature, because it is derived assuming that the cloud top is a black body and ignoring effects of the atmosphere above the cloud.
22. The 0.64-μm channel was corrected for sensor degradation [Y. J. Kaufman and B. N. Holben, *Int. J. Remote Sens.* **14**, 21 (1993); N. Che and J. C. Price, *Remote Sens. Environ.* **41**, 19 (1992)]. The on-board black bodies that emit thermal radiation in fixed temperatures are used to calibrate the 3.7- and 11-μm channels. The cloud reflectance at 3.7 μm, ρ_{c4}, was derived by subtracting the emissive part at 3.7 μm computed with T_{11} and correcting for attenuation and emission by water vapor derived from radiosonde data. Profiles of water vapor measured from radiosonde were obtained from the National Center for Atmospheric Research (obtained from D. Joseph, personal communication). In the analysis, the emissivity was assumed to be 1.0 at 11 μm and $1 - \rho_{c4}$ at 3.75 μm, because clouds selected by Eq. 1 are not transparent in these infrared channels (*13*). A sensitivity and validation study (*20*) indicates accuracy of the cloud droplet size for a similar method of ±2 μm and a precision that is better than that. τ_s is derived from the satellite-measured radiance over cloud-free, shadow-free pixels with dark vegetation cover (*13*, *34*) by means of a smoke optical model (*14*). Similar procedures applied to satellite data resulted in an uncertainty of $\Delta\tau_s \pm 0.1$ (*35*). For high optical thickness, an error of 20 to 30% is expected from uncertainty in the smoke-scattering phase function and single-scattering albedo.
23. A. Arking and J. D. Childs, *J. Climate. Appl. Meteorol.* **24**, 322 (1985).
24. W. R. Leaitch, G. A. Isaac, J. W. Strapp, C. M. Banic, H. A. Wiebe, *J. Geophys. Res.* **97**, 2463 (1992).
25. S. E. Schwartz and A. Slingo, *NATO ASI Series* **135**, 192 (1996).
26. S. A. Twomey, *J. Atmos. Sci.* **34**, 1149 (1977).
27. O. Boucher and T. L. Anderson, *J. Geophys. Res.* **100**, 26117 (1995).
28. T. C. Novakov, C. Rivera-Carpio, J. E. Penner, C. F. Rogers, *Tellus* **46B**, 132 (1994).
29. W. R. Leaitch *et al.*, *J. Geophys. Res.* **101**, 29103 (1996).
30. P. J. Crutzen *et al.*, *J. Atmos. Chem.* **2**, 233 (1985). For effects of convections see R. R. Dickerson *et al.*, *Science* **235**, 18473 (1987); V. W. J. H. Kirchhoff and E. V. A. Marinho, *Atmos. Environ.* **28**, 69 (1994); K. E. Pickering *et al.*, *J. Geophys. Res.* **101**, 23993 (1996).
31. The value determined by Penner *et al.* (*2*) of the global average indirect forcing by smoke could be an overestimate because (i) the study assumes a global homogeneous spatial distribution of the smoke aerosol in the presence of nonlinearity of the smoke effect; (ii) it neglects the presently observed low forcing for low availability of precipitable water vapor; and (iii) it neglects the production of smoke in the dry season with low cloud fraction.
32. T. R. Karl, R. W. Knight, G. Kukla, J. Gavin, in (*4*), pp. 363–384.
33. M. D. King, Y. J. Kaufman, P. Menzel, D. Tanre, *IEEE J. Geosci. Remote Sens.* **30**, 2 (1992); V. V. Salomonson, W. L. Barnes, P. W. Maymon, H. E. Montgomery, H. Ostrow, *ibid.* **27**, 145 (1989).
34. Y. J. Kaufman and C. Sendra, in *Aerosols and Climate*, P. V. Hobbs and M. P. McCormick, Eds. (Deepak, Hampton, VA, 1988), p. 51; B. N. Holben, E. Vermote, Y. J. Kaufman, D. Tanré, V. Kalb, *IEEE Trans. Geosci. Remote Sens.* **30**, 212 (1992); Y. J. Kaufman, in (*4*), p. 298.
35. R. S. Fraser, Y. J. Kaufman, R. L. Mahoney, *Atmos. Environ.* **18**, 2577 (1984); P. A. Durkee, D. R. Jensen, E. E. Hindman, T. H. Vonder Haar, *J. Geophys. Res.* **91**, 4063 (1986); P. A. Durkee, F. Pfeil, E. Frost, R. Shema, *Atmos. Environ.* **25a**, 2457 (1991); E. F. Vermote *et al.*, Special issue on Remote Sensing of Aerosol, *J. Geophys. Res.* **102**, 17131 (1997).
36. The satellite data were analyzed by S. Mattoo. The cloud detection was developed by M. Lawrence during a summer fellowship program at NASA Goddard Space Flight Center. We thank J. Tucker for assistance with AVHRR data and acknowledge valuable comments from O. Boucher, P. V. Hobbs, Y. Joseph, M. D. King, Z. Levin, J. E. Penner, S. Platnick, L. A. Remer, and D. Tanré.

29 May 1997; accepted 5 August 1997

Explosive Basaltic Volcanism from Cerro Negro Volcano: Influence of Volatiles on Eruptive Style

Kurt Roggensack,* Richard L. Hervig,† Steven B. McKnight,‡ Stanley N. Williams

The 1992 and 1995 basaltic eruptions of Cerro Negro volcano, Nicaragua, had contrasting eruptive styles. Although they were nearly identical in composition, the 1992 eruption was explosive, producing a 7-kilometer-high sustained ash column, whereas the 1995 eruption was essentially effusive. The differences in water and carbon dioxide contents of melt inclusions from the two eruptions define minimum saturation pressures and show how decompression of initially similar magmas influences eruptive style. Before eruption, the explosive 1992 magma retained water and carbon dioxide while ascending to a moderate crustal level (about 6 kilometers), whereas the nonexplosive 1995 magma lost all carbon dioxide by degassing during ascent to shallow crustal levels (about 1 to 2 kilometers).

Exsolution of water and carbon dioxide from erupting magmas provides the energy for explosive volcanism (*1*), but it has been difficult to correlate preeruptive volatile contents of magmas with eruption style (*2*) because factors such as conduit geometry, magma viscosity, and degassing history may also affect the explosivity of eruptions. Most earlier work has concentrated on silicic rather than basaltic explosive eruptions. Here, we contrast two recent eruptions of basaltic magma from the Cerro Negro volcano, Nicaragua, that show different eruptive styles, despite a common composition and vent geometry.

Cerro Negro is a small (~250 m high) basaltic volcano (Fig. 1) that has frequent but highly variable activity. The volcano's two most recent events highlight these differences. The April 1992 eruption, the first since 1971, was particularly energetic for a

Department of Geology, Box 871404, Arizona State University, Tempe, AZ 85287–1404, USA.

*To whom correspondence should be addressed.
†Also at Center for Solid State Science, Box 871704, Arizona State University, Tempe, AZ 85287–1704, USA.
‡Present address: Friends Seminary, 222 East 16 Street, New York, NY 10003, USA.